Banimohamad-Shotorbani et al., ***BioImpacts.*** 2025;15:30006
doi: 10.34172/bi.30006
https://bi.tbzmed.ac.ir/

Combination of mesenchymal stem cell sheet with poly-caprolactone nanofibrous mat and Gelfoam increased osteogenesis capacity in rat calvarial defect

Behnaz Banimohamad-Shotorbani[1,2], Reza Rahbarghazi[3,4*#], Seyedhosein Jarolmasjed[5], Ahmad Mehdipour[1], Hajar Shafaei[2,1,6*#]

[1]Department of Tissue Engineering, Faculty of Advanced Medical Sciences, Tabriz University of Medical Sciences, Tabriz, Iran
[2]Immunology Research Center, Tabriz University of Medical Sciences, Tabriz, Iran
[3]Stem Cell Research Center, Tabriz University of Medical Sciences, Tabriz, Iran
[4]Department of Applied Cell Sciences, Faculty of Advanced Medical Sciences, Tabriz University of Medical Sciences, Tabriz, Iran
[5]Department of Clinical Sciences, Faculty of Veterinary Medicine, University of Tabriz, Tabriz, Iran
[6]Department of Anatomical Sciences, Faculty of Medicine, Tabriz University of Medical Sciences, Tabriz, Iran
[#]The authors contributed equally to this work.

Article Info

Article Type:
Original Article

Article History:
Received: 17 Jul. 2023
Revised: 8 Oct. 2023
Accepted: 24 Oct. 2023
ePublished: 28 Apr. 2024

Keywords:
Mesenchymal stem cells, Cell sheet, Bone regeneration, Calvarial defects, Rat

Abstract

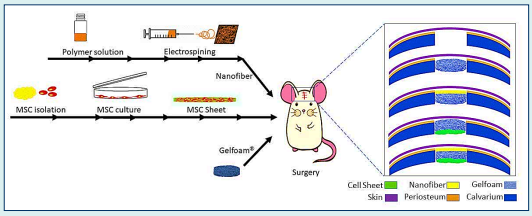

Introduction: To date, different strategies have been used for co-transplantation of cell-loaded biomaterials for bone tissue regeneration. This study aimed to investigate the osteogenic properties of adipose-derived-mesenchymal stem cell (AD-MSC) sheets combined with nanofibrous poly-caprolactone (PCL) mat and Gelfoam in rats with calvarial bone defect.

Methods: Calvarial critical-size defects were induced in male rats. Animals were classified into Control, Gelfoam, Gelfoam/PCL nanofiber, Gelfoam/AD-MSC sheet, and Gelfoam/PCL nanofiber/AD-MSC sheet groups. After 3 months, rats were sacrificed and the regeneration rate was evaluated.

Results: Almost all groups showed bone regeneration properties, but the volume of newly formed bone was higher in groups that received Gelfoam/AD-MSC and Gelfoam/PCL nanofiber/AD-MSC sheets ($P<0.05$). The application of Gelfoam/PCL nanofiber/AD-MSC sheets not only increased bone thickness, bone volume/total bone volume (BV/TV) ratio, strong Hounsfield Unit (HU), but also led to the formation of ossified connective tissue with wrinkled patterns.

Conclusion: The current study indicated that the Gelfoam/PCL nanofiber/AD-MSC sheet provides a suitable platform for effective osteogenesis in calvarial bone defects.

Introduction

Several pathological conditions such as trauma, tumors, inflammation, etc., can lead to progressive bone defects. To date, the reconstruction of bone defects is a challenging issue in clinical settings.[1] The craniofacial bone defect can influence the patient's health condition and also may cause difficulties in medical treatments. Although autograft and allograft substitutes are effective treatments for bone reconstruction they face some limitations such as morbidity of the donor site or the restricted availability of bone volume for transplantation purposes.[2,3] Besides, the osteogenic and osteoinductive properties of commercial grafts are poor and their applications cannot efficiently reconstruct large-size defects.[4] In this regard, bone tissue engineering is a promising and *de novo* therapeutic modality that attempts to eliminate the limitations and difficulties associated with traditional medication.[5] Nowadays, it has been indicated tissue engineering can appropriately restore the function of injured bone tissues via the combination of formulated biomaterials, stem cells, and several cytokines and growth factors.[6,7] In conventional tissue engineering, constructs are used as supporting platforms for transplanted cells for *in vivo* implantation purposes.[6,8] These strategies require

*Corresponding authors: Reza Rahbarghazi, Emails: rezarahbardvm@gmail.com, rahbarghazir@tbzmed.ac.ir, Hajar Shafaei, Email: shafaeih@tbzmed.ac.ir

specific biomaterials-based formulations with proper morphologies and physicochemical properties for efficient regenerative outcomes. For example, the existence of regulated porosity can contribute to suitable mechanical strength under load-bearing conditions,[9] supporting infiltration and dynamic growth of the seeded cells.[9,10] It was suggested that scaffolds with certain geometries dictate the differentiation of mesenchymal stem cells (MSCs) toward specific lineages.[11,12] Electrospun nanofibrous membranes are common scaffold types that are widely used for the fabrication of different types of natural and synthetic grafts.[13] Electrospun collagen nanofibrous membrane is an example that could mimic the natural osteogenic extracellular matrix (ECM) and promote bone regeneration.[8,14-16] Moreover, the electrospun nanofibers with a great surface area provide a favorable micro-environment for the adhesion and proliferation of cells. Of note, the role of topography and surface properties of scaffolds on stem cell fate is undeniable.[16]

To date, several synthetic and natural substrates have been used as electrospun nanofibers for tissue regeneration purposes,[17] with different synthesis protocols and formulas.[18] In clinical settings, electrospun nanofibers can be used as orthopedic fixation devices, drug delivery systems, resorbable sutures, and tissue engineering. It should be noted that polyesters are attractive members of synthetic polymers due to their optimal degradation rate and cytocompatibility.[19] Poly-caprolactone (PCL),[17,20] poly L-lactide and its copolymers,[17,21] chitosan,[22] silk fibroin,[23] etc, are commonly used in the fabrication of scaffolds with the potential to improve bone healing by promoting the proliferation and differentiation of seeded cells.[6] Polymers can be designed with favorable mechanical properties, degradation rates, and chemical functional groups that all can affect cell behavior and function.[19] PCL as a linear aliphatic polyester, flexible, hydrophobic,[17,24] nontoxic, low-cost,[8] osteogenic,[25] and biocompatible polymer, is one of the suitable candidates for tissue engineering.[24] Compared to the other polymers such as polyglycolic acid, polylactic acid, and poly lactide-co-glycolide, PCL possesses a suitable framework for bone regeneration due to its flexibility, long-term stability, and specific microenvironment that supports the primary coagulation of blood, infiltration of cells, and osteo-angiogenesis in a long time.[26,27] The high-rate toughness of PCL is due to its semi-crystalline structure at physiologic temperatures.[25] Besides, the promotion of physiologic endochondral ossification and chondrogenic differentiation are other advantages of PCL that lead to proper bone formation.[17]

In recent decades, cell sheet bioengineering appeared as a unique, efficient, and scaffold-free approach that keeps the cell-cell junctions via the production of native ECM.[28] Until now, several studies have been conducted to investigate the eligibility and efficacy of MSC sheets alone or in combination with biomaterials in craniofacial bone regeneration.[28] Ascorbic acid or vitamin C (Vit C) and dexamethasone (Dex) are two common agents that were used for MSC sheet bioengineering.[29,30] It is thought that the presence of Vit C not only leads to higher expression of mitogenic growth factors but also increases collagen type I (Col-I) secretion into the ECM.[31] Vit C in combination with Dex can stimulate Col-I/α2β1 integrin-mediated intracellular signaling.[32] Notably, the absence of Vit C reduces the expression of alkaline phosphatase (ALP) and also inhibits calcium deposition.[31] Along with these descriptions, Dex induces bone differentiation via the regulation of FHL2 expression. In support of this notion, the complete elimination of Dex from the human MSCs culture medium blunted differentiation capacity.[33] To be specific, the expression of Runx2 happens by Dex through FHL2/βcatenin-mediated transcriptional activation. Dex also could increase the activity of Runx2 by up-regulating TAZ and MKP1.[32] For calvarial defects, Gelfoam®, an FDA-approved gelatin-based sponge, is used as substrate for filling the defects. Gelfoam® has been extensively used as a wound dressing and contact hemostat to control bleeding in the surgical process.[34,35] Gelfoam® is a cost-effective, absorbable, porous, and sterile material that was obtained by boiling some tissues with water such as ligaments, tendons, bones, and skin.[34,35] In several studies, Gelfoam was used as a space filler,[36,37] delivery vehicle (a carrier matrix of cells[34,38] or exogenous cytokines,[39] a sealant of bone cement,[40] artificial periosteum,[41] an inhibitor of radial micro-movement of the bone scaffold,[42] and as a cellular scaffold to maintain the transplanted cells into the defect region without significant effect on osteogenesis.[34,43] Beside positive reports around MSC sheets, PCL, and Gelfoam® on calvarial surgeries, in the current study we investigated the efficacy of a novel triple construct including allogeneic rat AD-MSC (rAD-MSC) sheets, PCL electrospun membrane, and Gelfoam on regeneration of critical-size calvarial bone defects (CSD) in rats. It was hypothesized using combination form of these objects would gather effective properties of them so lead to enhanced bone regeneration (study groups containing double constructs would be more effective than single constructs). Especially, the expectation of the triple structure was more than the others (group containing triple construct would be effective than double and single constructs).

Materials and Methods

Materials

PCL, N, N-dimethylformamide tetrahydrofuran, tetrahydrofuran, and methyl thiazolyl tetrazolium were procurement from Sigma-Aldrich. DMEM/LG culture medium and Trypsin-EDTA solution were purchased from Gibco. Fetal bovine serum (FBS) was obtained from Biosera. Commercial Gelfoam® (Gelita-Spon, Gelita

Medical, Germany) was used in the current study.

Electrospun nanofiber production

Dimethylformamide and Tetrahydrofuran were used at a ratio of 1:1 to solve 0.6 g/9.5 ml PCL polymer. To prepare the homogeneous solution, the mixture was stirred for 12 hours and then placed into the syringe connected to a metal needle with an inner diameter of 0.3 mm. For electrospinning, a voltage of 25 kV was used. The space between the constant collector and the metal needle was adjusted to 14 cm and the flow rate was set to 2 mL/h. The surface of the collector was covered with aluminum foil to collect the nanofibers.[44]

Characterization of nanofibrous membrane

SEM analysis

To evaluate the microstructure of the nanofibrous membrane, a sample was prepared with an area of 5 mm × 5 mm after electrospinning. After gold sputtering, a scanning electron microscope (SEM; Model: Mira 3T scan, Philips XL30 ESEM) was used to analyze the surface of the nanofibrous membranes. ImageJ software was used to calculate the mean nanofiber diameter and pore size.[44] For this purpose, 100 random fibers were used for the calculation of mean nanofiber diameter.

Contact angle measurement

The contact angle measurement system (Dataphysics, OCA 15 plus) was used to assess wettability. The nanofibrous membrane was cut into a quadrangular shape and placed on the stage. About 4 µL distilled water drops were placed on the surface of the membrane by a motorized syringe at room temperature. The system included a CCD camera to calculate the contact angle using the images (analysis software PGX, Thwing-Albert Instrument Co., USA). This analysis was performed in triplicate random surface areas.[44]

Tensile strength analysis

The stress-strain test was applied using an Instron® machine (Model: Instron Z010, Zwick/Roell). The nanofibrous membrane was cut into a quadrangular shape (≈20 mm length × ≈5 mm width). The test was performed under the cross-head speed of 10 mm/min three times. Young's modulus was calculated using the equilibrium (Eq) 1[45]:

$$\text{Young modulus}\left(\text{E}\right)=\frac{\text{stress}\left(\sigma\right)}{\text{strain}\left(\varepsilon\right)} \qquad \text{Eq.}\left(1\right)$$

Animals

Adult male Wistar rats [8-week-old] weighing between 200-300 g were used for the isolation of stem cells and *in vivo* transplantation. This study was approved by the Local Research Ethics Committee of Tabriz University of Medical Sciences (Ethical code: IR.TBZMED.VCR.REC.1399.055). Rats were kept in standard cages under pathogen-free conditions with free access to chewing pellets and water. After one week, animals were used for *in vivo* analyses.

Cell isolation and expansion

rAD-MSCs were isolated and expanded as described according to standard protocols. Briefly, adipose samples were washed with PBS and digested enzymatically (collagenase I, 1 mg/mL) at 37°C. The pellet containing rAD-MSCs was obtained after centrifugation at 1300 rpm for 5 minutes, and cells were plated in cell culture flasks. rAD-MSCs were cultured in low-glucose content DMEM (DMEM/LG; Gibco) culture medium with 10% fetal bovine serum (FBS; Biosera) and 1% Penicillin-Streptomycin. Freshly isolated cells were maintained at 37°C under 5% CO_2 and 95% relative humidity. rAD-MSCs in passages 3-6 were used. In this study, 0.25% Trypsin-EDTA solution (Gibco) was applied to sub-culture the rAD-MSCs at 70-80% confluence.

MTT assay

The PCL nanofibers mats were punched roundly and sterilized under UV irradiation followed by floating in the 70% EtOH solution for 30 minutes. Then, samples were washed with phosphate-buffered saline (PBS) three times and placed on the bottom of 96-well plates. After that, about 3×10^3 rAD-MSCs were seeded in each well. The plates were maintained for 24, 48, and 72 hours under standard culture conditions. After the completion of incubation time, 20 µL methyl thiazolyl tetrazolium (MTT; dilution: 5 mg/mL; Sigma Aldrich) solution was added to each well and incubated at 37°C for 4 hours. The procedure was continued by supernatant removal and the addition of 100 µL DMSO solution to dissolve the formazan crystals. The viability of rAD-MSCs was evaluated by measuring the absorbance at 490 nm using a microplate reader (BioTek, Model: ELx808). The viability of rAD-MSCs in different groups was expressed as % of control cells plated on the plastic surface.[44]

Cell sheet fabrication

An approximate number of 5×10^5 rAD-MSCs were seeded in each well of 12-well plates and incubated in an osteogenesis medium supplemented with 10% FBS, 50 µg/mL Vit C, and 10 nM Dex.[46] Cells were maintained under these conditions until a confluent single rAD-MSC layer was achieved. The osteogenesis medium was replaced every 3-4 days. Imaging was done every few days to monitor sheet formation.[47] The cell sheet was harvested physically after two weeks using a cell scraper and assembled on the Gelfoam® sponge surface.

SEM imaging and H & E staining

The cell sheets were fixed using 2.5% glutaraldehyde

solution at 4°C for 24 hours and dried at room temperature. The imaging was performed after gold sputtering using SEM analysis as above-mentioned. We also performed an ultrastructural analysis of commercial Gelfoam® (Gelita-Spon, Gelita Medical, Germany). To see the microscopic thickness of the constructed cell sheet, H & E staining was performed as described previously.[47]

Implantation of constructs on calvarial bone

Fifteen rats were randomly placed into five groups (each in 3) as follows; Control, Gelfoam, Gelfoam/Nanofibers, Gelfoam/rAD-MSC sheet, and Gelfoam/Nanofibers/rAD-MSC sheet. In the current study, graft composition from the bottom to the top includes rAD-MSC sheet, Gelfoam, and PCL nanofibrous mat. In the control rats, calvarial defects were left untreated. After 12 hours of fasting, rats were anesthetized using halothane. For anesthesia induction, rats were exposed to inhale 3% halothane. The procedure was continued with the exposure of rats to 2% halothane for the maintenance of deep anesthesia. The procedure was done under a minimum alveolar concentration of 32%. Then, the skin was disinfected, and incised, and the native periosteum was removed to avoid simultaneous bone regeneration. The calvaria bone was exposed using trephine (~8 mm diameter) carefully under the extensive irrigation of sterile saline. The round full-thickness defects were performed on all animals in the same way. The same size prepared scaffolds were gently placed on the target sites and cutaneous tissue was sutured using 4-0 nylon strings. In postoperative care, animals received 8 mg/kg gentamicin and 1 mg/kg tramadol subcutaneously. Besides free access to water and food, all rats were observed and monitored diurnally for any complications or unusual behaviors during the three-month follow-up period. After that, animals were sacrificed after cardiorespiratory arrest using an overdose of sodium thiopental (Nesdonal®; 200 mg/kg) via the intraperitoneal route. The procedure was done according to the AVMA guidelines.

CBCT radiographic analysis

After a three-month follow-up, the calvarial bones were fixed in a 10% neutral buffered formalin solution and subjected to a scanner to take CBCT images using the NewTom VGi machine (Verona, Italy). A cone-shaped x-ray with a 360° rotation, 0.3-mm voxel size, and 18-second scan time at kVp = 110 was performed. The pixel size was 1920 × 1536 and the exposure condition was regulated automatically. 3D modeling of CBCT images was performed using mimics 21.0. (Materialise Leuven, Belgium). A round area (about 8 mm diameter) was placed in the central region of the initial defect area as the region of interest (ROI). The lateral view of newly formed bone/ROI was analyzed and applied contour surrounding. The new bone is also modeled inside the contours. For quantitative analysis, the volume of the demarcated defect region along with area, thickness, volume, and the Hounsfield unit (HU) of regenerated bone was assessed using mimics software.[48] The percentage of new bone volume (bone volume/total bone volume (BV/TV)) was calculated using Eq. 2. New bone area was performed using Eq.3.[49] The average bone thickness of five circular regions (4 points on each of the five regions) was compared qualitatively on the heat map.

$$New\ bone\ volume\ (\%) = \left(\frac{Volume\ of\ newly\ formed\ bone\ (BV)}{Total\ volume\ of\ defect\ region\ (TV)}\right) \times 100 \qquad Eq\ 2$$

$$New\ bone\ area\ (\%) = \left(\frac{Area\ of\ new\ bone}{Total\ area\ of\ the\ defect\ region}\right) \times 100 \qquad Eq\ 3$$

Histological analysis

After the completion of CBCT scanning, the fixed samples were dehydrated using an ascending concentration of ethanol, embedded in paraffin, and then cut into 5 µm thickness sections using a microtome.[50] Then, the H&E staining was performed on the specimens.

Raman spectroscopy

Molecular vibration of samples and Raman spectra were collected from 200-2000 (cm^{-1}) using a Raman spectrometer[51] (Handheld Raman Analyzer, Rigaku, FirstGuard) at the laser wavelength of 1064 nm. Samples were in the form of 20 µm thick sections on slides that were obtained using a microtome.

Statistical analysis

All data were reported as mean ± SD originating from three independent replicates. The statistical analysis was done based on ANOVA with post hoc Tukey using Graph Prism software version 8.02. P values < 0.05 were considered significant statistically. All assays were performed blindly.

Results

SEM imaging, contact angle, and tensile strength analyses

The SEM morphology of the electrospun PCL nanofibers is shown in Fig. 1A. Ultrastructural analysis revealed that PCL mats possess nano-sized fibrous structures ranging between 163 to 600 nm. To evaluate the wettability of PCL nanofibers, the water contact angle value was measured. An average water contact angle value of 121.5 degrees was achieved (Fig. 1B), indicating prominent hydrophobicity of developed PCL nanofibrous mats. To calculate the mechanical strength, the tensile stress of the electrospun nanofibrous PCL membrane was also determined. The stress-strain chart indicated that Young's modulus of the nanofibrous sheet reached 6.66 MPa with an ultimate tensile stress of 1.91 (Fig. 1C).

Survival rate of rAD-MSCs on the PCL nanofibrous mats

The cytocompatibility of the electrospun PCL nanofibrous was measured using an MTT assay at different time

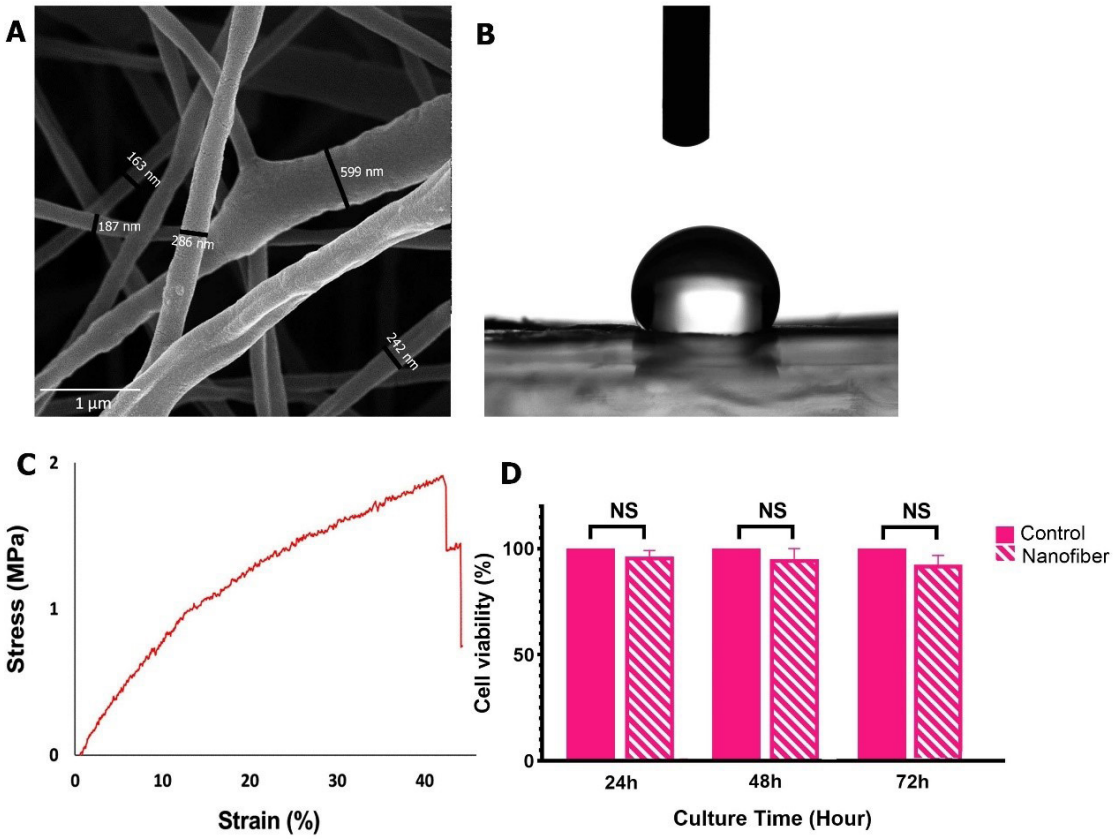

Fig. 1. SEM imaging of PCL nanofibrous membrane (A) Contact angel (B) and mechanical strength of nanofibrous PCL membrane (C). MTT assay revealed the lack of cytotoxicity in rAD-MSCs plated on the PCL nanofibers surface over 72 hours (D).

points (24, 48, and 72 hours). Data revealed the lack of cytotoxicity of PCL nanofibers at all-time points (Fig. 1D). Compared to the rAD-MSCs plated on the plastic surfaces, the culture of rAD-MSCs on PCL nanofibrous mats did not affect the survival rate after 72 hours, indicating the lack of possible cytotoxicity in the PCL scaffold.

Cell sheet formation and morphology

Bright-field imaging revealed the formation of a rAD-MSCs sheet after a 14-day culture time (Fig. 2A-E). The density of rAD-MSCs was increased over time and a single confluent rAD-MSC layer was achieved on day 14 (Fig. 2E). The physical detachment of confluent rAD-MSCs did not affect sheet structure (Fig. 2F). SEM imaging revealed that the rAD-MSC sheet represented a thin membrane with a tangled cellular network (Fig. 2G). Similarly, H & E staining indicated the existence of a close cell-to-cell network sheet structure after a 14-day (Fig. 2H). According to the data, the condensed matrix with a large number of rAD-MSCs can be detected in the lateral view of the sheet structure. A dense composition background indicates an appropriate production of ECM by rAD-MSCs. SEM analysis of Gelfoam was also performed in line with cell sheet analyses (Fig. 2I). Based on the data, numerous pores with suitable porosity were detected in the structure of Gelfoam.

Radiographic examination

To assess *de novo* bone formation at the target site, the regenerated region was modeled in 3D using CBCT files (based on performed defects (Fig. 3).

3D-reconstructive modeling of the regenerated bony area

According to the data, bone regeneration was observed in all study groups after 3 months compared to the control group. The larger area of bone formation was detected in the sequence of groups Gelfoam/rAD-MSC sheet (Fig. 4D) and Gelfoam/PCL nanofiber/rAD-MSC sheet (Fig. 4E) > Gelfoam/PCL nanofiber (Fig. 4C) > Gelfoam (Fig. 4B) > Control (Fig. 4A). These data exhibit the prominent osteogenic properties of the rAD-MSC sheet when transplanted simultaneously with Gelfoam. It was noted that the thickness of the regenerated region was in different groups. 3D modeling of target sites is shown in Fig. 4 rows i and ii. The coronal and sagittal views indicated the existence of radiopaque and radiolucent areas in the defect sites (Fig. 4F-J). Contour analysis revealed the radiopaque bone formation in the center of calvarial defects in rats that received Gelfoam/PCL nanofiber/rAD-MSC sheet while the application of Gelfoam/PCL nanofiber/rAD-MSC sheet induced *de novo* bone formation at the margins of defect areas. These data showed that the rAD-MSC sheets have a higher osteogenic capacity with Gelfoam compared

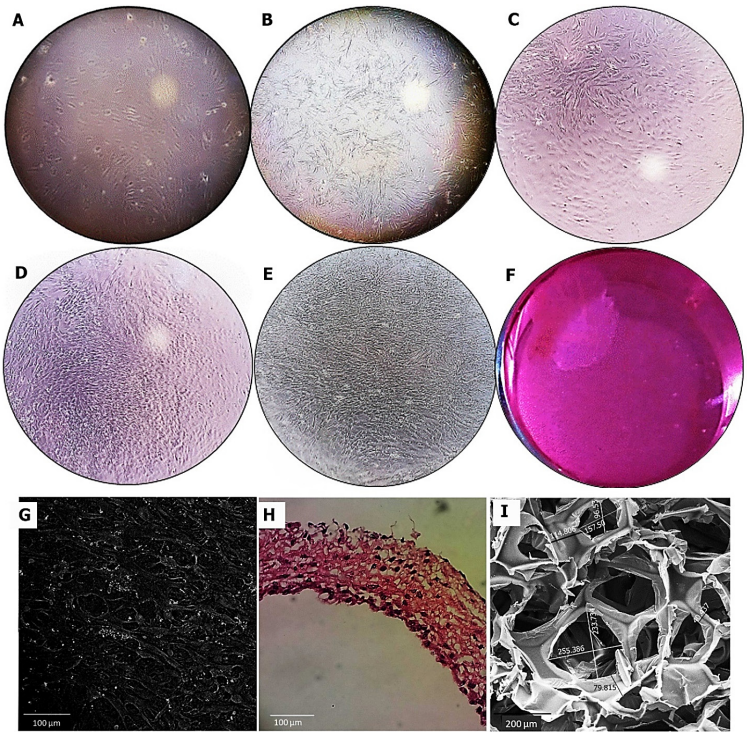

Fig. 2. In vitro culture of rAD-MSC for 14 days (A: day 2; B: day 5; C: day 8; D: day 11 and E: day 14). Bright-field images of rAD-MSCs culture led to the formation of a continuous sheet structure (A-E; Magnification: 4X; F: images taken from 15 cm of 6-well plates). SEM imaging confirmed close cell-to-cell interaction in the structure of the rAD-MSC sheet, scale bar: 100 µm (G). H & E staining showed the thickness rAD-MSC sheet structure with a dense ECM matrix. Scale bar: 100 µm (H). The porous view of the Gelfoam sponge was approved by SEM imaging, scale bar: 200 µm (I).

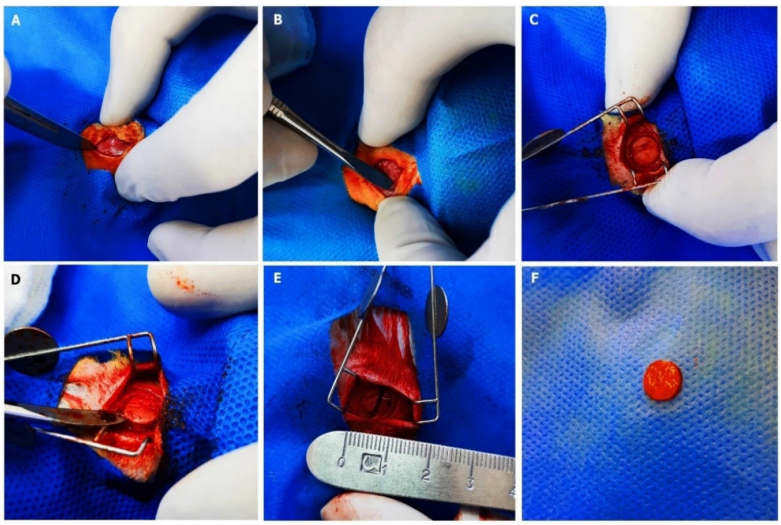

Fig. 3. Defect site. After cutting the skin of the target site (A) and removing the periosteum (B), an 8 mm diameter bone defect was induced (C), and the exposure and exclusion of bone (D-F).

Gelfoam/PCL nanofiber group. Of Note, the combination of Gelfoam and PCL nanofiber mat provides a platform to induce the activity of native osteoblasts in calvarial defects to deposit bone mineral components from the periphery of injured areas. Bone morphometric parameters such as the ratio of bone volume (BV)/total tissue volume (TV) were also calculated in this experiment (Fig. 5A). Data showed an increased BV/TV ratio in rats that received Gelfoam/rAD-MSC sheet and Gelfoam/PCL nanofiber/rAD-MSC sheet compared to the other groups (Fig. 5A; $P<0.05$). Non-significant differences were obtained in terms of the BV/TV ratio between the Gelfoam/rAD-MSC sheet and Gelfoam/PCL nanofiber/rAD-MSC sheet groups ($P>0.05$). The values of the BV/TV ratio in Control, Gelfoam, and Gelfoam/PCL nanofiber were about half of the other groups. Again, we found non-significant differences in the BV/TV ratio between the Control, Gelfoam, and Gelfoam/PCL nanofiber groups

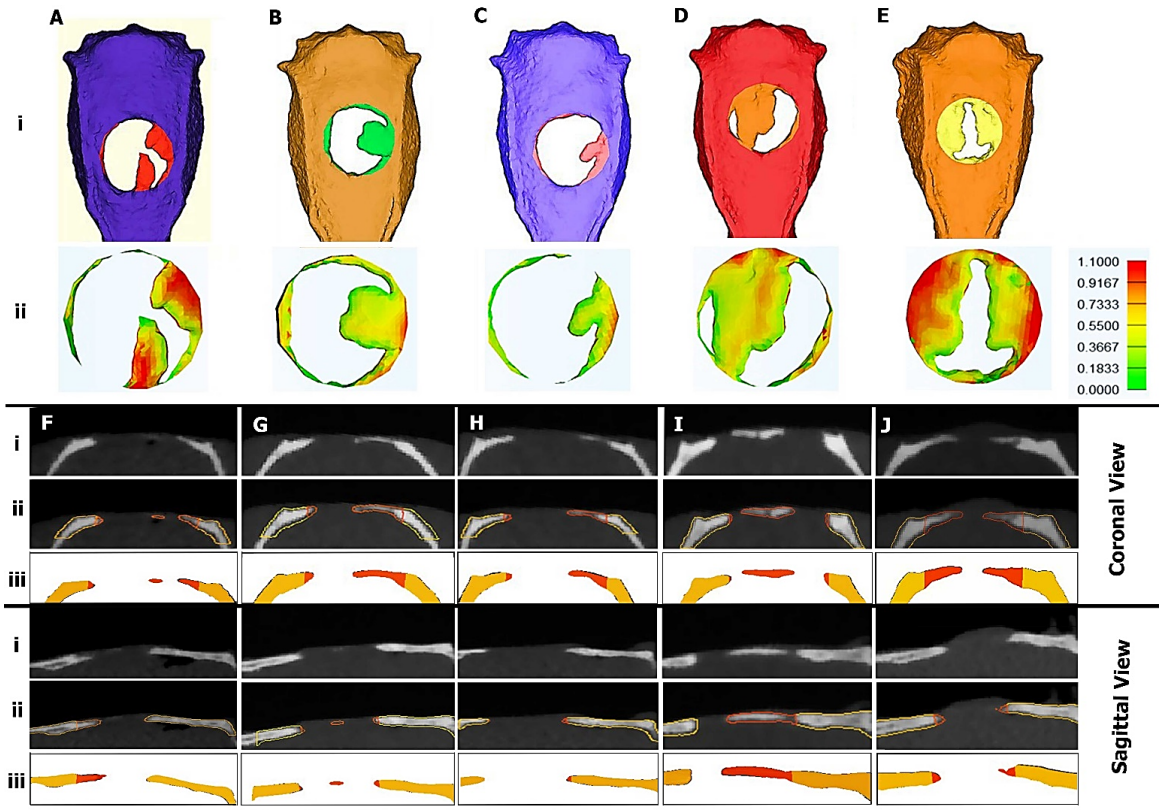

Fig. 4. 3D modeling of the CBCT pictures illustrated the defect region and regenerated bone [Control (Ai); Gelfoam (Bi); Gelfoam/PCL nanofiber (Ci); Gelfoam/rAD-MSC sheet (Di); and Gelfoam/PCL nanofiber/rAD-MSC sheet (Ei)]. The second row (ii) shows the thickness of new bone in correspondence groups. Panels from F to J demonstrate radiologic sections of correspondence groups in two views coronal and sagittal. The first row (i) showed simple images, the row ii showed the same views with contouring separated new and old bone. The red and yellow color of the contours showed new and old bone, respectively. Row iii showed modeled correspondence tissues. In the lateral view of the calvarium, radiopacity, and transparent regions were seen at the defects. Using contour, host and newly formed bone was evident separately (F-J). Coronal and sagittal views of regenerated defects were shown in three rows. The first row (i) showed the radiologic image of the calvarial. In the second row (ii), old and new bones were shown with contour, and the third row (iii) showed 3D modeling of upper rows with old and new bones.

(Fig. 5A; $P>0.05$). The area is considered as the two-dimensional parameter that avoids the role of thickness. Non-significant differences were found in terms of area (%) in all groups (Fig. 5B). Relative radiodensity analysis (HU) revealed higher values in Gelfoam/PCL nanofiber/rAD-MSC sheet groups compared to the other groups ($P<0.05$). Transplantation of the Gelfoam/rAD-MSC sheet did not yield significant HU values compared to the Control, Gelfoam, and Gelfoam plus PCL nanofiber groups ($P<0.05$). According to the heat map analysis, peripheral sites of newly formed bone were the thickest parts. From peripheral regions to central parts, the thickness of new bone was decreased. Qualitative analysis indicated that rats that received rAD-MSC sheets in combination with Gelfoam and PCL nanofibers exhibited newly thick bone formation (Fig. 5D).

Histologic evaluation

Bright-field imaging revealed that the calvarial defects were left empty in control rats after 12 weeks (Fig. 6A). Histological examination revealed bone regeneration at the peripheral region of the defect coincided with thin, loose connective tissue and three or four layers of cells. Data indicated intramembranous ossification and the progression of the periosteum in the control group. Compared to the control rats, higher loose connective tissue with irregular collagen fibers can be detected in the Gelfoam group (Fig. 6B). The pattern of bone formation in the Gelfoam group is similar to the control group. In the Gelfoam/PCL nanofiber group, thick, high-rate cell density with more heterogeneous connective tissue and a wrinkled pattern can be detected (Fig. 6C). Based on the data, connective tissue was covered with periosteum which is the continuation of the adjacent bone tissue periosteum. It seems that immature newly formed bone had numerous round-shaped cells with irregular Haversian systems. In defects filled with Gelfoam/rAD-MSC sheet, higher amounts of connective tissue with parallel collagen fibers were indicated (Fig. 6D). However, the new bone with round cells was immature, and Haversian systems were at primary stages. Again, ossification was observed in the growing edges. The transplantation of the Gelfoam/PCL nanofiber/rAD-MSC sheet led to the formation of ossified connective tissue with wrinkled patterns (Fig. 6E). Microscopic analysis indicated highly heterogeneous cellularity with thicker connective tissue in comparison

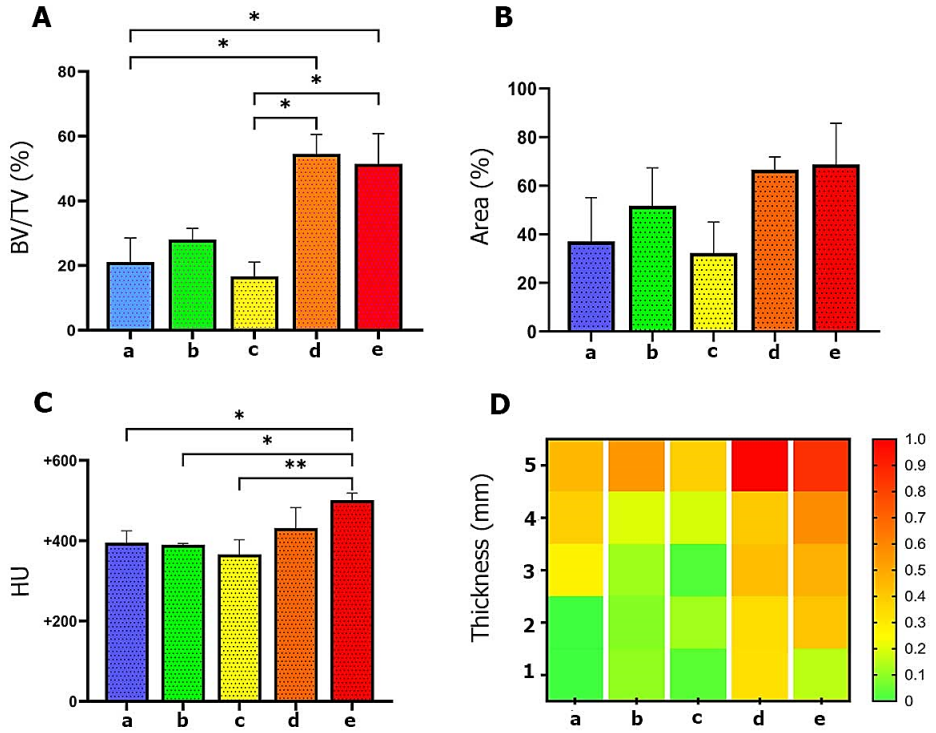

Fig. 5. Percentage of new bone volume to total bone volume at the defect region (A). Bone area (B). Hounsfield unit of new bones (C). The heat map chart showed the qualitative comparison between groups a-e (D). The regions of defect were described by numbers from the center to peripheral parts (ring-like areas starting from the center to the periphery). Number 1 referred to the center of the defect, and number 5 referred to the most peripheral ring. According to the colors, the peripheral regions were the thickest in all groups. Groups d and e (containing rAD-MSC sheets) looked thicker than the others. One-way ANOVA with post hoc Tukey; * $P<0.05$, and ** $P<0.01$).

with the other groups. The newly formed bone was immature with high cell densities. Based on the data, it seems that ossification occurred primarily at the bottom surface and continued to the top layers.

Raman spectroscopy

Raman spectroscopy was used to obtain data about the molecular structure of newly formed bone. The analysis was done in approximate ranges within the molecular vibration associated with bone structure.[52] The molecular vibration of generated regions is shown in Fig. 6A-E. The bands in the range of ≈ 957-962 $cm^{-1,}$ 422–454 $cm^{-1,}$ and 568–617 were associated with υ1 stretching of the P-O bond, υ2 bending of the O-P-O, and υ4 bending of phosphate tetrahedral (PO_4^{-3}) respectively [53] that are represented on the spectrums with blue color (Fig. 6). The band of $CO3^{-2}$ was indicated around 1065-1071 cm^{-1} in light red color. Bands of collagen matrix included bonds of proline ≈ 851-855 cm^{-1} (purple color), hydroxyproline ≈ 870-873 cm^{-1} (light green color), Amide III ≈ 1200-1320 cm^{-1} (light purple color), C-H (CH_2 deformation is related to protein wagging) ≈ 1447-1452 cm^{-1} with light pink highlight, and amide I ≈ 1595-1720 cm^{-1} at yellow highlight.[52-55]

Discussion

In the current study, we investigated the osteogenic properties of allogeneic AD-MSC sheets in the form of different constructs in rats with CSD. It has been elucidated that the reparative effects of MSCs in the reconstitution of bone defects are associated with paracrine activity, differentiation capacity toward target cell lineages, and regulation of immune cell function.[1,3,56] Compared to the direct and static seeding of the cells on the surface of scaffolds or onto the substrates, the application of cell sheet technology can help us to transplant more cell numbers into the defect sites. It is believed that secreted ECM by cells could act as a potent regulator of cellular function and differentiation after transplantation into the injured bone areas.[57] Cell sheet technology using MSC sheets alone or in combination with other biomaterials is an eligible approach to accelerate the healing of bone defects.[57] As reported before, the application of both Vit C and Dex significantly can increase the expression of Col-I, osteocalcin, and proteoglycan, and this strategy is more efficient when cells are closely attached within the sheet structure.[58] The critical role of ECM on osteoblast differentiation was previously indicated by Xiao and co-workers. It was suggested that the close interaction between cell integrins (α2β1) and surrounding ECM components such as Col-I is initiated. Inside the cells, the activation of relevant downstream signaling pathways such as MAPK2 and Runx2 phosphorylation contributes to osteoblast differentiation.[32,59] The existence of organized ECM in

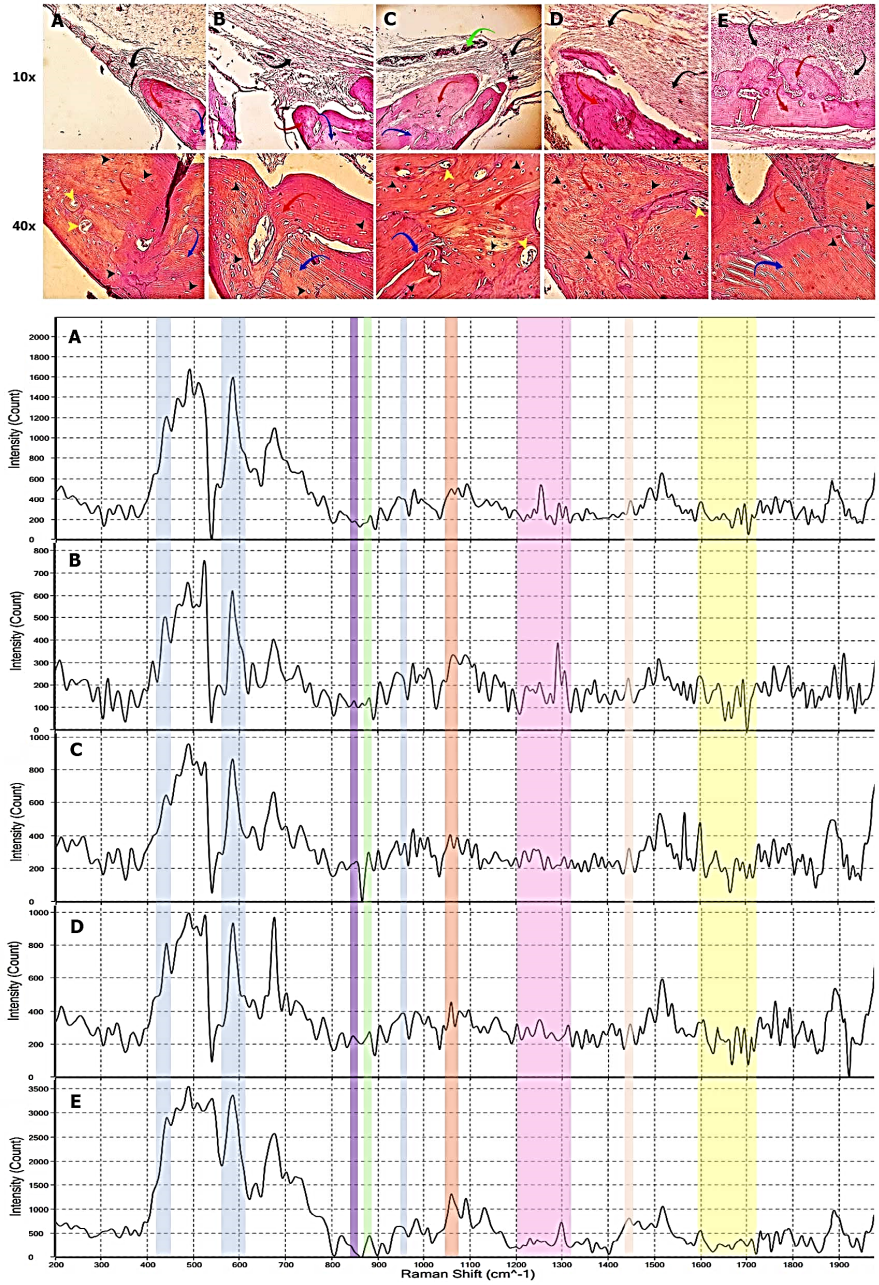

Fig. 6. Histologic views and spectroscopy of new bone. The upper part of the figure showed H & E staining at the magnification of 10X and 40X. The black arrows: are connective tissues; the red arrows: are newly formed bone; the blue arrows: are old (host) bone; the green arrows: are the remains of the Gelfoam; the black head arrows: are osteocytes in lacunae (there were some empty lacunae); and the yellow head arrow: the Haversian canals. The lower part compared spectrums of new bone at the defect regions. The new bone of all groups showed molecular vibration information of phosphate (light blue highlights), Amide I and III (yellow and light purple highlights), Carbonate (light red highlight), collagen matrix (purple and light green highlight), and deformation of protein (light pink highlight).

the cell sheet structure not only could affect transplanted MSCs differentiation potential but also probably affect the activity of host osteoblasts to form the new bone units.

In this study, we used MSC sheet units in combination with Gelfoam and Gelfoam/PCL membrane in rats with CSD. As reported previously, Gelfoam is a hemostatic agent and can preserve the osteogenic potential of cells.[34,60] According to our results and related previous reports, Gelfoam alone had no significant effect on bone regeneration. Therefore, one could hypothesize that Gelfoam acts as a hemostat and physical platform that facilitates the attachment of MSC sheets to the target sites. It was shown that co-administration of the Gelfoam sponge and PCL nanofibrous membrane led to lower osteogenic properties. One reason would be related to the specific entity of Gelfoam and PCL nanofibrous mats with high hydrophilicity and hydrophobicity which were reported previously by previous studies.[43,61] Besides, rapid degradation of PCL can affect regenerative outcomes. Of note, a rapid mass loss of PCL-based scaffolds has been

reported from 0 to 3 months after transplantation into the target sites.[62] Zhang et al showed that the higher porosity and surface area could lead to a higher hydrolysis rate and acid byproduct production.[63] The co-administration of Gelfoam and its artificial clot might prevent the easy diffusion of PCL degradation products.[64,65] So, acidic products aggregate at the internal surface of the defect site and possibly make tissue regeneration difficult. As the usage of Gelfoam is common during surgical procedures, the authors proposed to notice the synergic effect of Gelfoam with other biomaterials in terms of bone formation. Gelfoam and PCL are two safe and effective materials however simultaneous transplantation did not yield a regenerative outcome. In other groups, the combination of Gelfoam/MSC sheet and Gelfoam/MSC sheet/PCL membrane was applied for induction bone formation. To date, several strategies have been used for the successful production of cellular sheets.[6,46,56,66,67] Previously, N-isopropyl acryl amide-methacrylic acid hydrogel was used as a thermo-responsive polymer to harvest the cell sheet through temperature reduction below the lower critical solution temperature of the copolymers.[47] In this study, a more straightforward method, a cell scraper, was used to harvest the cell sheet structure. Consistent with other experiments; the present data suggested that placement of MSC sheets on the bone injury sites significantly enhances new bone formation.[3,6,29,68,69] The co-transplantation of rAD-MSC sheets with Gelfoam and PCL nanofibers led to higher HU, and BV/BT ratios compared to groups that received Gelfoam alone and Gelfoam/PCL nanofiber mat. It was shown that PCL nanofibrous mats can increase the density of regenerated bone.[70] Along with data from a study conducted by Zhang et al, both transplanted MSC sheets and host tissue cells successfully participated in the formation of *de novo* bone units.[71] It should not be forgotten that native and intact ECM in the form sheet structure can increase the osteogenic activity of laden stem cells before and after transplantation.[59] According to data from the H & E staining panel, intramembranous bone formation was detected at the edge of defect regions. The construction of new bone units continued from the inner areas of the skull to the outer areas. By the activation of the osteogenic process, the rAD-MSC sheet can be gradually degraded by the artificial clot and thus PCL membrane-derived acidic degradation products are diffused. The degradation of ECM compounds such as proteins and glycoproteins is one of the biological functions of MMPs secreted by transplanted stem cells.[72-74] It has been indicated that MMPs function in several biologic processes such as migration, cell mobility, etc.[72] Lozito et al claimed that the secretion of MMP-2 and -10 by AD-MSCs increases cell migration and ECM remodeling.[75] These features can stimulate the migration of stem cells and native osteoblasts toward the injured sites and relatively reduce the disadvantages of Gelfoam/PCL nanofibers. Besides these effects, the release of several signaling biomolecules via MSC-derived exosomes can also accelerate osteogenesis.[76,77] Using Raman spectroscopy, non-destructive screening of chemical composition and microstructure of target tissues became possible.[55] In this technique, vibrational details and information were provided based on scattered monochromatic laser light.[52] The numerate of scattered photons are peaks of the spectrum and the intensity of peaks shows the concentrations of a particular chemical bond.[78] Information on the collagen backbone can be achieved based on two spectral bonds of amide groups (I and III).[78,79] Amide I bonds exhibit carbonyl stretching (1560 and 1725 cm^{-1}). Two vibrational modes were responsible for the bond of amide III, including stretching and bending. The first one was related to stretching between carbon and nitrogen atoms, and the second one was the bending of a secondary amine (1210 and 1350 cm^{-1}).[78] As amide bonds are involved in the backbone of collagen, loss of relative intensity (at 1245 cm^{-1}) is integral to collagen fragmentation.[78] The main distinct mineral bond in the bone spectrum is phosphate stretching at 960 cm^{-1}.[78] Under poorly-preservation conditions, the peaks of amide III, I, and CH_2 were remarkably reduced, but inorganic-related peaks remained unchanged, indicating protein degradation.[80] Notably, a reduction of the peak intensity of amide III was reported in those specimens that were maintained under poor preservation.[78] In *de novo* bone units similar typical peaks of bone tissue can be indicated due to appropriate bone mineralization.[51,78] All results obtained from Raman spectroscopy results were aligned with the previous studies.[78-80]

Here, we faced some limitations that need to be addressed in future studies. Only three rats were allocated to each experimental group. An adequate sample size, at least six animals per group, can improve scientific validity and accuracy. It is suggested that therapeutic properties of varied stem cell types such as bone marrow and umbilical cord MSCs be examined in terms of cell sheet technology and osteogenesis.

Research Highlights

What is the current knowledge?

√ Stem cell sheets have been used as a novel cell-based therapeutic approach in bone tissue engineering.

What is new here?

√ Combination of MSC-sheet with PCL nanofibers, and Gelfoam improved bone regeneration in rats with calvarial bone defect.

Conclusion

In summary, this study showed the osteogenic potential

of the rAD-MSC sheet in combination with Gelfoam and PCL nanofibers in rat CSD. It seems that the rAD-MSC sheet could reduce the negative synergic effect of Gelfoam/PCL nanofibers on bone formation. The presence of the rAD-MSC sheets beside PCL nanofiber and Gelfoam improved bone regeneration and HU index. In short, this study proposes the usage of cell sheets as a potentially efficient cell-based therapeutic option for calvarial bone reconstruction in the clinical setting.

Acknowledgments
Authors wish to thank the personnel of Faculty of Advanced Medical Sciences for guidance and help.

Authors' Contribution
Conceptualization: Hajar Shafaei.
Formal analysis: Behnaz Banimohamad-Shotorbani.
Funding acquisition: Hajar Shafaei.
Investigation: Behnaz Banimohamad-Shotorbani.
Methodology: Ahmad Mehdipour, Seyedhosein Jarolmasjed.
Project administration: Hajar Shafaei, Reza Rahbarghazi.
Supervision: Hajar Shafaei, Reza Rahbarghazi.
Validation: Hajar Shafaei, Reza Rahbarghazi.
Writing—original draft: Behnaz Banimohamad-Shototrbani.
Writing—review & editing: Reza Rahbarghazi.

Competing Interests
The authors declare that they have no conflict of interest.

Ethical Statement
All phases of this study were approved by the Local Ethics Committee of Tabriz University of Medical Sciences under the ethical code of Ethical code: IR.TBZMED.VCR.REC.1399.055).

Funding
This is a report of the database from a Ph.D. thesis registered in Tabriz University of Medical Sciences with grant number of 64739 under the supervision of Dr. Hajar Shafaei.

References
1. Ma D, Ren L, Chen F, Liu Y, Zhang J, Xue Z, *et al.* Reconstruction of rabbit critical-size calvarial defects using autologous bone marrow stromal cell sheets. *Ann Plast Surg* **2010**; 65: 259-65. https://doi.org/10.1097/SAP.0b013e3181c9c3f5.
2. Fretwurst T, Gad LM, Nelson K, Schmelzeisen R. Dentoalveolar reconstruction: modern approaches. *Curr Opin Otolaryngol Head Neck Surg* **2015**; 23: 316-22. https://doi.org/10.1097/MOO.0000000000000167.
3. Liu Y, Wang H, Dou H, Tian B, Li L, Jin L, *et al.* Bone regeneration capacities of alveolar bone mesenchymal stem cells sheet in rabbit calvarial bone defect. *J Tissue Eng* **2020**; 11: 2041731420930379. https://doi.org/10.1177/2041731420930379.
4. Eppley BL, Pietrzak WS, Blanton MW. Allograft and alloplastic bone substitutes: a review of science and technology for the craniomaxillofacial surgeon. *J Craniofac Surg* **2005**; 16: 981-9. https://doi.org/10.1097/01.scs.0000179662.38172.dd.
5. Seddighian A, Ganji F, Baghaban-Eslaminejad M, Bagheri F. Electrospun PCL scaffold modified with chitosan nanoparticles for enhanced bone regeneration. *Prog Biomater* **2021**; 10: 65-76. https://doi.org/10.1007/s40204-021-00153-8.
6. Ren Z, Ma S, Jin L, Liu Z, Liu D, Zhang X, *et al.* Repairing a bone defect with a three-dimensional cellular construct composed of a multi-layered cell sheet on electrospun mesh. *Biofabrication* **2017**; 9: 025036. https://doi.org/10.1088/1758-5090/aa747f.
7. Saghati S, Nasrabadi HT, Khoshfetrat AB, Moharamzadeh K, Hassani A, Mohammadi SM, *et al.* Tissue Engineering Strategies to Increase Osteochondral Regeneration of Stem Cells; a Close Look at Different Modalities. *Stem Cell Rev Rep* **2021**; 17: 1294-311. https://doi.org/10.1007/s12015-021-10130-0.
8. Shin M, Yoshimoto H, Vacanti JP. In vivo bone tissue engineering using mesenchymal stem cells on a novel electrospun nanofibrous scaffold. *Tissue Eng* **2004**; 10: 33-41. https://doi.org/10.1089/107632704322791673.
9. Farajpour H, Bastami F, Bohlouli M, Khojasteh A. Reconstruction of bilateral ramus-condyle unit defect using custom titanium prosthesis with preservation of both condyles. *J Mech Behav Biomed Mater* **2021**; 124: 104765.
10. Nazarov R, Jin H-J, Kaplan DL. Porous 3-D scaffolds from regenerated silk fibroin. *Biomacromolecules* **2004**; 5: 718-26. https://doi.org/10.1016/j.jmbbm.2021.104765.
11. Metavarayuth K, Sitasuwan P, Zhao X, Lin Y, Wang Q. Influence of surface topographical cues on the differentiation of mesenchymal stem cells in vitro. *ACS Biomater Sci Eng* **2016**; 2: 142-51. https://doi.org/10.1021/acsbiomaterials.5b00377.
12. Watari S, Hayashi K, Wood JA, Russell P, Nealey PF, Murphy CJ, *et al.* Modulation of osteogenic differentiation in hMSCs cells by submicron topographically-patterned ridges and grooves. *Biomaterials* **2012**; 33: 128-36. https://doi.org/10.1016/j.biomaterials.2011.09.058.
13. Karkan SF, Davaran S, Rahbarghazi R, Salehi R, Akbarzadeh A. Electrospun nanofibers for the fabrication of engineered vascular grafts. *J Biol Eng* **2019**; 13: 83. https://doi.org/10.1186/s13036-019-0199-7.
14. Liao S, Li B, Ma Z, Wei H, Chan C, Ramakrishna S. Biomimetic electrospun nanofibers for tissue regeneration. *Biomed Mater* **2006**; 1: R45-53. https://doi.org/10.1088/1748-6041/1/3/R01.
15. Jang J-H, Castano O, Kim H-W. Electrospun materials as potential platforms for bone tissue engineering. *Adv Drug Deliv Rev* **2009**; 61: 1065-83. https://doi.org/10.1016/j.addr.2009.07.008.
16. Abagnale G, Steger M, Nguyen VH, Hersch N, Sechi A, Joussen S, *et al.* Surface topography enhances differentiation of mesenchymal stem cells towards osteogenic and adipogenic lineages. *Biomaterials* **2015**; 61: 316-26. https://doi.org/10.1016/j.biomaterials.2015.05.030.
17. Yao Q, Cosme JG, Xu T, Miszuk JM, Picciani PH, Fong H, *et al.* Three dimensional electrospun PCL/PLA blend nanofibrous scaffolds with significantly improved stem cells osteogenic differentiation and cranial bone formation. *Biomaterials* **2017**; 115: 115-27. https://doi.org/10.1016/j.biomaterials.2016.11.018.
18. Zander NE. Hierarchically structured electrospun fibers. *Polymers* **2013**; 5: 19-44. https://doi.org/10.3390/polym5010019.
19. Gunatillake PA, Adhikari R, Gadegaard N. Biodegradable synthetic polymers for tissue engineering. *Eur Cell Mater* **2003**; 5: 1-16. https://doi.org/10.22203/ecm.v005a01.
20. Rezaei H, Shahrezaee M, Monfared MJ, Karkan SF, Ghafelehbashi R. Simvastatin-loaded graphene oxide embedded in polycaprolactone-polyurethane nanofibers for bone tissue engineering applications. *J Polym Eng* **2021**; 41: 375-86. https://doi.org/10.1515/polyeng-2020-0301.
21. Stachewicz U, Qiao T, Rawlinson SC, Almeida FV, Li W-Q, Cattell M, *et al.* 3D imaging of cell interactions with electrospun PLGA nanofiber membranes for bone regeneration. *Acta Biomater* **2015**; 27: 88-100. https://doi.org/10.1016/j.actbio.2015.09.003.
22. Ehterami A, Khastar H, Soleimannejad M, Salehi M, Nazarnezhad S, Majidi Ghatar J, *et al.* Bone Regeneration in Rat using Polycaprolactone/Gelatin/Epinephrine Scaffold. *Drug Dev Ind Pharm* **2022**; 2021;47: 1915-1923. https://doi.org/10.1080/03639045.2022.2070640.
23. Xiang J, Li Y, Ren M, He P, Liu F, Jing Z, *et al.* Sandwich-like nanocomposite electrospun silk fibroin membrane to promote osteogenesis and antibacterial activities. *Appl Mater Today* **2022**; 26: 101273. https://doi.org/10.1016/j.apmt.2021.101273.
24. Pae HC, Kang JH, Cha JK, Lee JS, Paik JW, Jung UW, *et al.* 3D-printed polycaprolactone scaffold mixed with β-tricalcium phosphate as a bone regenerative material in rabbit calvarial defects. *J Biomed Mater Res B Appl Biomater* **2019**; 107: 1254-63. https://doi.org/10.1002/jbm.b.34218.

25. Dwivedi R, Kumar S, Pandey R, Mahajan A, Nandana D, Katti DS, *et al.* Polycaprolactone as biomaterial for bone scaffolds: Review of literature. *J Oral Biol Craniofac Res* **2020**; 10: 381-8. https://doi.org/10.1016/j.jobcr.2019.10.003.
26. Byun J-H, Lee HAR, Kim TH, Lee JH, Oh SH. Effect of porous polycaprolactone beads on bone regeneration: preliminary in vitro and in vivostudies. *Biomater Res* **2014**; 18: 1-8. https://doi.org/10.1186/2055-7124-18-18.
27. Low S, Ng Y, Yeo T, Chou N. Use of Osteoplug polycaprolactone implants as novel burr-hole covers. *Singapore Med J* **2009**; 50: 777-80.
28. Chen G, Qi Y, Niu L, Di T, Zhong J, Fang T, *et al.* Application of the cell sheet technique in tissue engineering. *Biomed Rep* **2015**; 3: 749-57. https://doi.org/10.3892/br.2015.522.
29. Ma D, Ren L, Yao H, Tian W, Chen F, Zhang J, *et al.* Locally injection of cell sheet fragments enhances new bone formation in mandibular distraction osteogenesis: a rabbit model. *J Orthop Res* . **2013**; 31: 1082-8. https://doi.org/10.1002/jor.22336.
30. Nakamura A, Akahane M, Shigematsu H, Tadokoro M, Morita Y, Ohgushi H, *et al.* Cell sheet transplantation of cultured mesenchymal stem cells enhances bone formation in a rat nonunion model. *Bone* **2010**; 46: 418-24. https://doi.org/10.1016/j.bone.2009.08.048.
31. Vater C, Kasten P, Stiehler M. Culture media for the differentiation of mesenchymal stromal cells. *Acta biomate* **2011**; 7: 463-77. https://doi.org/10.1016/j.actbio.2010.07.037.
32. Langenbach F, Handschel J. Effects of dexamethasone, ascorbic acid and β-glycerophosphate on the osteogenic differentiation of stem cells in vitro. *Stem Cell Res Ther* **2013**; 4: 1-7. https://doi.org/10.1186/scrt328.
33. Hamidouche Z, Haÿ E, Vaudin P, Charbord P, Schüle R, Marie PJ, *et al.* FHL2 mediates dexamethasone-induced mesenchymal cell differentiation into osteoblasts by activating Wnt/β-catenin signaling-dependent Runx2 expression. *FASEB J* **2008**; 22: 3813-22. https://doi.org/10.1096/fj.08-106302.
34. Wofford A, Bow A, Newby S, Brooks S, Rodriguez R, Masi T, *et al.* Human fat-derived mesenchymal stem cells xenogenically implanted in a rat model show enhanced new bone formation in maxillary alveolar tooth defects. *Stem Cell Int* **2020**; 2020: 8142938. https://doi.org/10.1155/2020/8142938.
35. Ashour A, Zaghloul M, Mahmoud W, Helal M, Grawish M. Gelfoam haemostatic agent with or without autologous bone marrow-derived stem cells for the regeneration of critical-size mandibular defects in the rabbit. *Int J Oral Maxillofac Surg* **2018**; 47: 1488-94. https://doi.org/10.1016/j.ijom.2018.04.021.
36. Khairy MA, Sabry D, Mostafa S. The effect of adipose derived stem cells on bone regeneration in mandibular cavity defects. *Egypt Dent J* **2020**; 61: 1-11.
37. Kandel F, Atef M, Asker N. Maxillary sinus elevation using gelfoam (absorbable gelatin) versus xenograft (Tutogen) with simultaneous implant placement (randomized clinical trial). *Dent J* **2018**; 64: 1475.
38. Mesgarzadeh AH, Nasiri I, Jarolmasjed S, Naghibi M, Shafaei H. Evaluation of bone regeneration in mandible large defect using undifferentiated adipose stem cells loaded on gelatin carrier: An animal model case study. *J Dent Res Dent Clin Dent Prospects* **2021**; 15: 22. https://doi.org/10.34172/joddd.2021.005.
39. Akita S, Fukui M, Nakagawa H, Fujii T, Akino K. Cranial bone defect healing is accelerated by mesenchymal stem cells induced by coadministration of bone morphogenetic protein-2 and basic fibroblast growth factor. *Wound Repair Regen* **2004**; 12: 252-9. https://doi.org/10.1111/j.1067-1927.2004.012118.x.
40. Ahn J-M, Oh J-S. Gelfoam embolization technique to prevent bone cement leakage during percutaneous vertebroplasty: comparative study of gelfoam only vs. gelfoam with venography. *Korean J Neurotrauma* **2020**; 16: 200. https://doi.org/10.13004/kjnt.2020.16.e42.
41. Lee J-Y, Choi M-H, Shin E-Y, Kang Y-K. Autologous mesenchymal stem cells loaded in Gelfoam® for structural bone allograft healing in rabbits. *Cell Tissue Bank* **2011**; 12: 299-309. https://doi.org/10.1007/s10561-010-9194-4.
42. K Kwon J, Lee DJ, Kocher M, Kim Y-I, Wu T-J, Whitley J, *et al.* The inhibition of radial and axial micromovement of bone scaffold with gelfoam® and titanium mesh fixation and its effects on osteointegration. *Methods Protoc* **2019**; 2: 20. https://doi.org/10.3390/mps2010020.
43. Ponticiello MS, Schinagl RM, Kadiyala S, Barry FP. Gelatin-based resorbable sponge as a carrier matrix for human mesenchymal stem cells in cartilage regeneration therapy. *J Biomed Mater Res* **2000**; 52: 246-55. https://doi.org/10.1002/1097-4636(200011)52:2<246::aid-jbm2>3.0.co;2-w.
44. Karkan SF, Rahbarghazi R, Davaran S, Kaleybar LS, Khoshfetrat AB, Heidarzadeh M, *et al.* Electrospun polyurethane/poly (ε-caprolactone) nanofibers promoted the attachment and growth of human endothelial cells in static and dynamic culture conditions. *Microvasc Res* **2021**; 133: 104073. https://doi.org/10.1016/j.mvr.2020.104073.
45. Alharbi N, Daraei A, Lee H, Guthold M. The effect of molecular weight and fiber diameter on the mechanical properties of single, electrospun PCL nanofibers. *Mater Today Commun* **2023**; 35: 105773. https://doi.org/10.1016/j.mtcomm.2023.105773.
46. Wang X, Li G, Guo J, Yang L, Liu Y, Sun Q, *et al.* Hybrid composites of mesenchymal stem cell sheets, hydroxyapatite, and platelet-rich fibrin granules for bone regeneration in a rabbit calvarial critical-size defect model. *Exp Ther Med* **2017**; 13: 1891-9. https://doi.org/10.3892/etm.2017.4199.
47. Shotorbani BB, André H, Barzegar A, Zarghami N, Salehi R, Alizadeh E. Cell sheet biofabrication by co-administration of mesenchymal stem cells secretome and vitamin C on thermoresponsive polymer. *J Mater Sci Mater Med* **2018**; 29: 1-17. https://doi.org/10.1007/s10856-018-6180-z.
48. Khojasteh A, Safiaghdam H, Farajpour H. Pedicled segmental rotation techniques for posterior mandible augmentation: a preliminary study. Int J Oral Maxillofac Surg ***2019***; 48(12):1584-1593. https://doi.org/10.1016/j.ijom.2019.04.009.
49. Pothuaud L, Van Rietbergen B, Mosekilde L, Beuf O, Levitz P, Benhamou CL, *et al.* Combination of topological parameters and bone volume fraction better predicts the mechanical properties of trabecular bone. *J Biomech* **2002**; 35(8):1091-9. https://doi.org/10.1016/s0021-9290(02)00060-x.
50. Hassani A, Khoshfetrat AB, Rahbarghazi R, Sakai S. Collagen and nano-hydroxyapatite interactions in alginate-based microcapsule provide an appropriate osteogenic microenvironment for modular bone tissue formation. *Carbohydr Polym* **2022**; 277: 118807. https://doi.org/10.1016/j.carbpol.2021.118807.
51. Suenaga H, Furukawa KS, Suzuki Y, Takato T, Ushida T. Bone regeneration in calvarial defects in a rat model by implantation of human bone marrow-derived mesenchymal stromal cell spheroids. *J Mater Sci Mater Med* **2015**; 26: 1-9. https://doi.org/10.1007/s10856-015-5591-3.
52. Khalid M, Bora T, Ghaithi AA, Thukral S, Dutta J. Raman spectroscopy detects changes in bone mineral quality and collagen cross-linkage in staphylococcus infected human bone. *Sci Rep* **2018**; 8: 1-9. https://doi.org/10.1038/s41598-018-27752-z.
53. Ahmed R, Law AWL, Cheung TW, Lau C. Raman spectroscopy of bone composition during healing of subcritical calvarial defects. *Biomed Opt Express* **2018**; 9: 1704-16. https://doi.org/10.1364/BOE.9.001704.
54. Kozielski M, Buchwald T, Szybowicz M, Błaszczak Z, Piotrowski A, Ciesielczyk B. Determination of composition and structure of spongy bone tissue in human head of femur by Raman spectral mapping. *J Mater Sci Mater Med* **2011**; 22: 1653-61. https://doi.org/10.1007/s10856-011-4353-0.
55. Buchwald T, Kozielski M, Szybowicz M. Determination of collagen fibers arrangement in bone tissue by using transformations of Raman spectra maps. *J Spectrosc* **2012**; 27: 107-17. https://doi.org/10.1155/2012/261487.
56. Xie Q, Wang Z, Huang Y, Bi X, Zhou H, Lin M, *et al.*

Characterization of human ethmoid sinus mucosa derived mesenchymal stem cells (hESMSCs) and the application of hESMSCs cell sheets in bone regeneration. *Biomaterials* **2015**; 66: 67-82. https://doi.org/10.1016/j.biomaterials.2015.07.013.
57. Li D, Wang W, Guo R, Qi Y, Gou Z, Gao C. Restoration of rat calvarial defects by poly (lactide-co-glycolide)/hydroxyapatite scaffolds loaded with bone mesenchymal stem cells and DNA complexes. *Chin Sci Bull* **2012**; 57: 435-44. https://doi.org/10.1007/s11434-011-4914-0.
58. Akahane M, Shimizu T, Kira T, Onishi T, Uchihara Y, Imamura T, *et al.* Culturing bone marrow cells with dexamethasone and ascorbic acid improves osteogenic cell sheet structure. *Bone Joint Res* **2016**; 5: 569-76. https://doi.org/10.1302/2046-3758.511.BJR-2016-0013.R1.
59. Xiao G, Gopalakrishnan R, Jiang D, Reith E, Benson MD, Franceschi RT. Bone morphogenetic proteins, extracellular matrix, and mitogen-activated protein kinase signaling pathways are required for osteoblast-specific gene expression and differentiation in MC3T3-E1 cells. *J Bone Miner Res* **2002**; 17: 101-10. https://doi.org/10.1359/jbmr.2002.17.1.101.
60. Dudas JR, Marra KG, Cooper GM, Penascino VM, Mooney MP, Jiang S, *et al.* The osteogenic potential of adipose-derived stem cells for the repair of rabbit calvarial defects. *Ann Plast Surg* **2006**; 56: 543-8. https://doi.org/10.1097/01.sap.0000210629.17727.bd.
61. D Dash TK, Konkimalla VB. Polymeric modification and its implication in drug delivery: poly-ε-caprolactone (PCL) as a model polymer. *Mol Pharm* **2012**; 9: 2365-79. https://doi.org/10.1021/mp3001952.
62. Lam CX, Hutmacher DW, Schantz JT, Woodruff MA, Teoh SH. Evaluation of polycaprolactone scaffold degradation for 6 months in vitro and in vivo. *J Biomed Mater Res A* **2009**; 90: 906-19. https://doi.org/10.1002/jbm.a.32052.
63. Zhang Q, Jiang Y, Zhang Y, Ye Z, Tan W, Lang M. Effect of porosity on long-term degradation of poly (ε-caprolactone) scaffolds and their cellular response. *Polym Degrad Stab* **2013**; 98: 209-18. https://doi.org/10.1016/j.polymdegradstab.2012.10.008.
64. Guralnick WC. Absorbable gelatin sponge and thrombin in oral surgery. *Am J Orthod* **1946**; 32: 792-4. https://doi.org/10.1016/0096-6347(46)90041-5.
65. Guralnick WC, Berg L. Gelfoam in oral surgery: a report of two hundred fifty cases. *Oral Surg Oral Med Oral Pathol* **1948**; 1: 632-9. https://doi.org/10.1016/0030-4220(48)90337-5.
66. Kobayashi J, Kikuchi A, Aoyagi T, Okano T. Cell sheet tissue engineering: cell sheet preparation, harvesting/manipulation, and transplantation. *J Biomed Mater Res A* **2019**; 107: 955-67. https://doi.org/10.1002/jbm.a.36627.
67. Uchiyama H, Yamato M, Sasaki R, Sekine H, Yang J, Ogiuchi H, *et al.* In vivo 3D analysis with micro-computed tomography of rat calvaria bone regeneration using periosteal cell sheets fabricated on temperature-responsive culture dishes. *J Tissue Eng Regen Med* **2011**; 5: 483-90. https://doi.org/10.1002/term.340.
68. Shi L, Tee BC, Cotter L, Sun Z. Enhance Mandibular Symphyseal Surface Bone Growth with Autologous Mesenchymal Stem Cell Sheets: An Animal Study. *Aesthetic Plast Surg* **2020**; 44: 191-200. https://doi.org/10.1007/s00266-019-01494-3.
69. Mu S, Tee B, Emam H, Zhou Y, Sun Z. Culture-expanded mesenchymal stem cell sheets enhance extraction-site alveolar bone growth: An animal study. *J Periodontal Res* **2018**; 53: 514-24. https://doi.org/10.1111/jre.12541.
70. Yoshida Y, Matsubara H, Fang X, Hayashi K, Nomura I, Ugaji S, *et al.* Adipose-derived stem cell sheets accelerate bone healing in rat femoral defects. *PLoS One* **2019**; 14: e0214488. https://doi.org/10.1371/journal.pone.0214488.
71. Zhang W, Xue D, Yin H, Wang S, Li C, Chen E, *et al.* Overexpression of HSPA1A enhances the osteogenic differentiation of bone marrow mesenchymal stem cells via activation of the Wnt/β-catenin signaling pathway. *Sci Rep* **2016**; 6: 1-11. https://doi.org/10.1038/srep27622.
72. Laronha H, Caldeira J. Structure and function of human matrix metalloproteinases. *Cells* **2020**; 9: 1076.
73. Ries C, Egea V, Karow M, Kolb H, Jochum M, Neth P. MMP-2, MT1-MMP, and TIMP-2 are essential for the invasive capacity of human mesenchymal stem cells: differential regulation by inflammatory cytokines. *Blood* **2007**; 109: 4055-63. https://doi.org/10.1182/blood-2006-10-051060.
74. Uder C, Brückner S, Winkler S, Tautenhahn HM, Christ B. Mammalian MSC from selected species: Features and applications. *Cytometry A* **2018**; 93: 32-49. https://doi.org/10.1002/cyto.a.23239.
75. Lozito TP, Jackson WM, Nesti LJ, Tuan RS. Human mesenchymal stem cells generate a distinct pericellular zone of MMP activities via binding of MMPs and secretion of high levels of TIMPs. *Matrix biology* **2014**; 34: 132-43.
76. Chen S, Tang Y, Liu Y, Zhang P, Lv L, Zhang X, *et al.* Exosomes derived from miR-375-overexpressing human adipose mesenchymal stem cells promote bone regeneration. *Cell Proliferation* **2019**; 52: e12669. https://doi.org/10.1016/j.matbio.2013.10.003.
77. Mianehsaz E, Mirzaei HR, Mahjoubin-Tehran M, Rezaee A, Sahebnasagh R, Pourhanifeh MH, *et al.* Mesenchymal stem cell-derived exosomes: a new therapeutic approach to osteoarthritis? *Stem Cell res Ther* **2019**; 10: 1-13. https://doi.org/10.1186/s13287-019-1445-0.
78. France CA, Thomas DB, Doney CR, Madden O. FT-Raman spectroscopy as a method for screening collagen diagenesis in bone. *J Archaeol Sci* **2014**; 42: 346-55. https://doi.org/10.1016/j.jas.2013.11.020.
79. B Barth A, Zscherp C. What vibrations tell about proteins. *Q Rev Biophys* **2002**; 35: 369-430. https://doi.org/10.1017/s0033583502003815.
80. McLaughlin G, Lednev IK. Potential application of Raman spectroscopy for determining burial duration of skeletal remains. *Anal Bioanal Chem* **2011**; 401: 2511-8. https://doi.org/10.1007/s00216-011-5338-z.